Lama Hamadeh, Amin Al-Habaibeh, Towards Reliable Smart Textiles: Investigating Thermal Characterisation of Embedded Electronics in E-Textiles Using Infrared Thermography and Mathematical Modelling, Sensors and Actuators A: Physical ,2022,113501,ISSN 0924-4247; Available on line at: https://doi.org/10.1016/j.sna.2022.113501

Towards Reliable Smart Textiles: Investigating Thermal Characterisation of Embedded Electronics in E-Textiles Using Infrared Thermography and Mathematical Modelling

Lama Hamadeh[1] and Amin Al-Habaibeh[2*]

[1] Mechanical Engineering Department

Faculty of Engineering Sciences

University College London, London, UK

[2]Product Innovation Centre

Nottingham Trent University

Nottingham, UK

Abstract

The smart textiles field, which includes e-textiles, has seen rapid development in recent years due to its wide market applications such as wearables, architecture, energy and product design. Electronic circuits of e-textiles involve devices such as LEDs, sensors and batteries that are embedded within the yarns. Since temperature is a crucial element causing profound problems to the electronic devices when it exceeds a certain threshold, extensive research efforts have to be done to reduce its negative effect and enhance the sustainability of such embedded devices. In this work, infrared thermographic imaging technology is utilised to experimentally study the thermal distribution profile of LEDs in their bare, encapsulated and embedded state in e-yarns manufacturing stages. The experimental results are compared with numerical analysis models carried out when solving the time-dependent and partial differential equations of the heat transfer process. In this work, infrared camera with 320x240 pixel vanadium oxide microbolometer that detects temperature differences of less than 0.1^{o}K is utilised with a special micro close-up lens to take close-up infrared images of the LED samples. Additionally a point-measurement technique, using a thermocouple, is utilised to ensure accurate temperature measurements are recorded for calibration. The results of this work prove that using infrared thermography with suitable lens can provide significant information about the thermal behaviour of smart textiles. It has been found that the thermal distribution of the integrated LEDs has a Gaussian-like shape. This bell-shaped distribution gets higher and wider by adding an additional LED device to the circuit within a specific distance range. It has been found that in the case of multiple LEDs, the distance between them plays a crucial role in determining the overall temperature of the system and shaping the final overall thermal distribution, and hence the reliability of the smart textile on the long term. The results also show that the cover yarn can influence the heat dissipation process. Consequently, the selection of yarn's material and structure could be a critical factor to the thermal performance of electronic devices embedded within e-textiles.

Keywords:

Infrared thermography, electronic components, smart textile; electronic textiles; architecture; e-textiles; wearable technologies.

* Corresponding author: Professor Amin Al-Habaibeh, Nottingham Trent University, email: amin.al-habaibeh@ntu.ac.uk, Tel: 0115 848 2564.

List of variables:

Variable	Definition
I	Electric current (A)
V	Electric voltage (V)
R	Resistance (Ohm)
P	Electric power (W)
$P_{\text{electrical}}$	Electric power produced by LED (W)
P_{heat}	Heat generation by LED (W)
P_{optical}	LED optical output power (W)
η_{LED}	LED efficiency (%)
L	LED length (mm)
T	Temperature (^{o}C)
x	Distance (mm)
α	Thermal diffusivity (mm^2/s)
d	Distance between two LEDs (mm)
$\overline{T_{1,2}}(\bar{x},\bar{t})$	Temperature functions for each LED individually (^{o}C)
$\bar{T}_{\text{Total}}(\bar{x},\bar{t})$	The total solution of the system's temperature (^{o}C)
$\psi_{1,2}(\bar{x},\bar{t})$	Modified temperature functions for each LED individually (^{o}C)
$\psi_{\text{Total}}(\bar{x},\bar{t})$	Modified total solution of the system's temperature (^{o}C)
$\lambda_{1,2,3,4}$	Correction functions
$s_{1,2}$	$\lambda_{1,2}$ parameters
$\gamma_{1,2}$	
$h_{1,2}$	

1. Introduction

The growth of smart textiles that include electronic textiles (e-textiles) and wearable technologies is revolutionising the way people connect through smart devices, hence having a great impact on the textile and fashion industries. The future of wearable fabrics as we usually know them as something to wear to provide coverage, convey our sense of style and protect us from the environmental elements is about to change in an immense way; and smart textiles are paving the way for this change. Smart textiles have the ability to do various tasks that traditional fabrics cannot, including data capturing and communication, light illumination and transformation of energy. This would improve peoples' everyday lifestyle and benefit the industry, the health care sector and the environment.

Textiles, in addition to being wearable, have a wide range of applications [1], this includes for example aeronautics [2], buildings architecture [3, 4] and medical applications [5]. The integration of multifunctional values in textiles has become a special area of interest in recent years [6,7,8]. Fibres yarns, fabric and other structures with added-value functionality have been developed for a range of applications, such as: energy management [9, 10], energy harvesting [11], fabric heaters [12], memory [13], sensors [14,15,16,17,18], communication [19, 20], health [21,22,23,24,25, 26] and motion monitoring [27, 28] based on electronic devices within the fabric to facilitate the human-device interaction

Electronic devices have seen a huge improvement in the past decades in the textile industry as well as other sectors. For example, electronic devices, such as sensors are now integrated to textiles as well as 3D printed using additive manufacturing. Reference [29] has covered recent 3D printing technology and development for electronic components; where it has suggested that current research should provide enhanced and optimised fabrication as well as more sensitive products. Other papers [30] have presented scalable carbon nanotube-based textile as distributed sensors to provide data for condition monitoring of the manufacturing process as well as structural health monitoring during operation.

In principle, e-textile circuits contain classical electronic devices, such as LEDs, in addition to conventional batteries embedded into garments. The demand for reliable operation of electronic devices in a wide range of applications and in all types of environmental conditions drives the need to define the potential problem areas in electronic circuits design and propose new methods and ideas to improve their performance. For wearable e-textile, one of the major causes of failures is mechanical stress of washing [31]. Other research which has covered this area is [32] and indicated that time, temperature and mechanical stresses from washing influences the reliability.

Various studies have also identified temperature as a major cause of failure of electronic systems in all applications. For example, [33] indicated that operating at 80^{o}C will reduce life time by 65% when compared to operating at 40^{o}C. Reference [34] used infrared thermography and modelling to explore the effect of temperature on electronic devices. [35] has indicated that temperature is the main cause of reduce reliability of electronic devices that is attributed to a combination of various physical and chemical processes. Such high level of temperatures might not be merely ambient temperatures, but more related to localised temperatures at the centre of the small electronic devices if heat dissipation is not efficient.

In this paper, the objective of this study is in assessing the operational temperature of electronic devices used in e-textiles with the focus on LEDs. A novel approach of using mathematical modelling and infrared thermography is used to assess the thermal performance and evaluate the relationship between yan

manufacturing and the thermal profile as well as the proximity of the electronic devices and the effect on the thermal profile. This is addressed as part of the reliability studies.

Generally, at any instant, the power P (watts) consumed by an electronic component with resistance R (ohm) is calculated as: $P = I^2R = I\,V = V^2/R$, where: V (volts) is the voltage across the electronic component, and I (amps) is the current flowing through it. Using Ohm's law, the two other forms can be derived. Part of this power is converted into heat which must be dissipated via the electronic component's package before its temperature rises excessively so that the temperature all over the system remains acceptable and within suitable levels. In the case of LED devices, the amount of heat generated as a result of the electric power depends essentially on the LED efficiency, η_{LED}. Based on the law of energy conservation, the input electrical power, $P_{\mathrm{electrical}}$, can be divided into two main parts; one is the optical output power, P_{optical}, and the other is heat generation, P_{heat} [36]:

$$P_{\mathrm{electrical}} = P_{\mathrm{heat}} + P_{\mathrm{optical}} \tag{1}$$

Hence, the optical efficiency of the LED can be defined as:

$$\eta_{\mathrm{LED}} = \frac{P_{\mathrm{optical}}}{P_{\mathrm{electrical}}} \qquad \text{or} \qquad 1 - \eta_{\mathrm{LED}} = \frac{P_{\mathrm{electrical}} - P_{\mathrm{optical}}}{P_{\mathrm{electrical}}} \tag{2}$$

Three different efficiencies η_{LED} for the LED can be considered:

1. $\eta_{\mathrm{LED}} = 1$:

This is the ideal case of LED where no heat is generated in the LED, and the total electric power is transferred into optical power, i.e., light.

2. $0 < \eta_{\mathrm{LED}} < 1$

This is the general case for any LED in nowadays market. The electric power that goes through the LED has two components: thermal and optical. Hence, the efficiency of the LED depends on the proportion that each component has. For example, if the LED's efficiency is 65%, this means that 65% of the electric power is transferred into an optical energy, i.e., light; and the remaining 35% is transferred into thermal energy, i.e., heat. This leads to a rise in LED's temperature. It is worth mentioning that in this project we use LED samples that has efficiency $\eta_{\mathrm{LED}} = 50\%$.

3. $\eta_{\mathrm{LED}} = 0$

When the LED's efficiency is zero, then the entire electric power is transferred into thermal energy and no optical energy is produced. Practically speaking, this is a pointless case as it describes an unproductive LED which acts mainly as a resistive load.

Infrared (IR) thermography is an important and a widely-used thermal and non-contact evaluation tool utilised to get information in temperature-dependent applications such as crowd monitoring [37], aerospace [38], health [39 , 40], buildings [41], microwave circuits [42], food [43] and manufacturing [44] industries to accurately measure in real time and visualise the temperature profile of the studied systems. With the advent of newer generations of infrared cameras, infrared thermography is becoming more accurate, reliable and cost-effective technique [45]. Indeed, today a vast variety of infrared imaging devices is available, allowing also measurements in complex configurations such as in the presence of fast phenomena or moving objects [46]. As a 2D imaging technique, infrared thermography provides a straightforward approach to map the entire temperature distribution on a whole area of interest and produces a thermal image where the colour-map represent ranges of temperatures, and allowing the extraction of pixel-by-pixel temperatures. Therefore, using infrared thermography in this work to analyse the thermal behaviour of LED electronic devices that are integrated into e-textiles, helps in understanding their thermal profile towards enhancing their performance and advancing their multi-functionality.

The aim of this research work is to study and analyse, experimentally by using infrared thermography imaging and theoretically by solving numerically the time-dependent heat transfer equation, the thermal dissipation profile of LEDs embedded in e-textiles and draw a comparison between both results towards providing information to the manufacturers and developers towards understanding the thermal performance and enhancing long term reliability.

This paper is organised as follows: after the introduction in section 1, the mathematical modelling and numerical analysis of the system are presented in section 2. In section 3, the infrared experimental methodology and results are described. The discussion and conclusion to this work is reviewed in sections 4 and 5 respectively. We conclude with the acknowledgements in section 6.

2. Mathematical Modelling

In the analysis and the quest for the understanding of a physical system, generally, the formulation and use of a mathematical model that is thought to describe the system is an essential step. Generally, simulation and thermal modelling is a very important step to go along with the experimental work as it gives a full description and understanding of the response and performance of a physical system and its logical behaviour predictions at limits that might not be experimentally possible. In this section, a numerical analysis for the thermal dissipation mechanism of the LED and its corresponding solutions are provided. Mainly, considering solving the one-dimensional, time-dependent and partial differential equation of the heat transfer in MATLAB software using finite difference discretisation method for one LED and for two LEDs with different separation distance, d , between them.

2.1 The modelling system

In this study, as shown in Figure 1, a simplified circuit is considered that contains a rectangular LED with length L, a power supply, a copper wire and a switch. At $t = 0$, in Figure 1-a, the circuit's switch is closed and connected to a power supply with a voltage $V(\text{Volts})$ and an electric current $I(\text{Amps})$ which goes through the circuit. Generally speaking, at any instant, the power P (watts) consumed by any electric component with resistance $R(\text{ohm})$ is calculated by [47]: $P = I^2R = I\,V = V^2/R$. The LED's temperature in this case is homogenous (uniform) at its maximum, i.e., $T_1 = T_{\max}$. Since the heat source will be at the semiconductor junction in the middle and heat will spread externally, at steady state the LED is expected to have the same uniform or homogeneous temperature. To observe the temperature dissipation (diffusion) along the LED, the circuit switch is made open, in Figure 1-b, where the electric current stops going through the circuit and therefore neither optical nor thermal energy is generated.

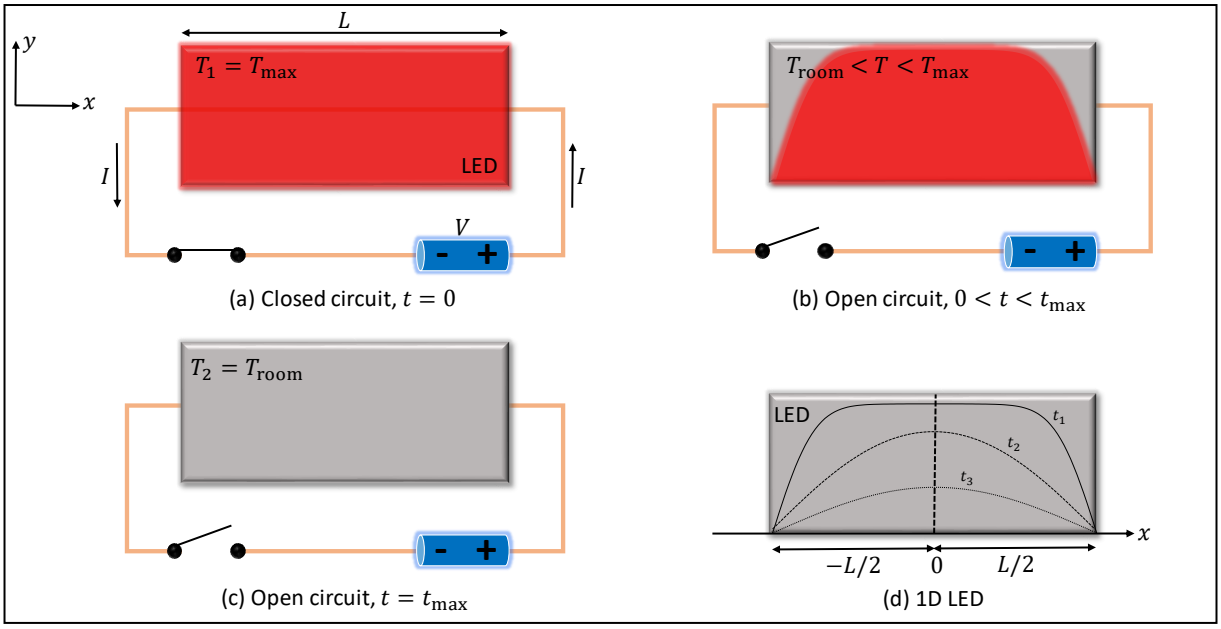

Figure 1: Simplified schematics illustrating the thermal distribution within the LED at $t = 0$ in (a) when the electronic circuit is closed, at $0 < t < t_{max}$ in (b) and at $t = t_{max}$ in (c) when the circuit is open. (d) is the 1D LED along x axis with the thermal distributions at times $t_1 < t_2 < t_3$ are presented along the LED.

The LED's temperature begins to gradually decreases by time, i.e., $T_{room} < T < T_{max}$, where the centre of the LED cools more slowly than the points near the ends. The thermal distribution keeps dissipating until the LED's overall temperature is equivalent to the room temperature, i.e., $T_2 = T_{room}$ at $t = t_{max}$ as shown in Figure 1-c. Here, we will develop a simplified model for the thermal distribution within the LED that is connected to a power supply with an electric power P at $t = 0$ and simulate the behaviour of its time-dependent thermal distribution after the circuit is disconnected from the power supply.

2.2 One-dimensional time-dependent heat transfer equation

Heat transfer is energy in transit due to a temperature difference. One of the methods that heat can transfer from one medium to another is conduction. In the presence of a temperature gradient, energy transfer by conduction must occur in the direction of decreasing temperature [48]. Generally, the heat transfer equation, or the so-called diffusion equation (or Fourier's or Fick's second law), in a stationary and homogeneous medium is a parabolic, time-dependent, linear and partial differential equation and is given by [47]:

$$\frac{\partial T(x,t)}{\partial t} = \alpha \nabla^2 T(x,t) \tag{3}$$

Where $T(x,t)$ is the temperature in space-time point, $x(\mathrm{m})$ is the space, $t(\mathrm{sec})$ is the time, $\alpha(\mathrm{m}^2.\mathrm{sec}^{-1})$ is the thermal diffusivity[1], and $\nabla^2 = \partial^2/\partial x^2 + \partial^2/\partial y^2 + \partial^2/\partial z^2$ is the Laplacian operator. Equation (3) is three dimensional, but using the Cartesian coordinates, the one-dimensional version of this equation becomes

$$\frac{\partial T(x,t)}{\partial t} = \alpha \frac{\partial^2 T(x,t)}{\partial x^2} \tag{4}$$

The temperature field remains symmetrical about the mid-plane of the LED because the boundary conditions are identical at both surfaces, as shown in Figure 1-d. The x coordinate origin can then be placed at the centre

[1] Thermal diffusivity is a property that measures the ability of a material to conduct energy relative to its ability to store energy. Materials with large α will respond more quickly to changes in their thermal environment, while materials with a small α will respond more slowly, taking longer to reach a new equilibrium condition. Thermal diffusivity is given by: $\alpha = \frac{k}{\rho c}$ where: k is the thermal conductivity $(\mathrm{W.m^{-1}.K^{-1}})$, ρ is the density $(\mathrm{Kg.m^{-3}})$ and c is the specific heat capacity $(\mathrm{J.Kg^{-1}.K^{-1}})$ [47].

of the LED assuming that the temperature distribution is symmetrical about the mid-plane. Also, the adiabatic condition can be imposed at $x = 0$. The boundary conditions of the problem and the initial condition are then:

$$\left.\frac{\partial T}{\partial x}\right|_{x=0} = 0$$
$$T\left(x = -\frac{L}{2}, t\right) = T\left(x = \frac{L}{2}, t\right) = T_1 = T_{\text{room}} \quad (5)$$
$$T_0(x, t = 0) = T_2 = T_{\max}$$

To numerically analyse the temperature distribution in the LED, we use the PDE solver in MATLAB to solve the partial differential equation of the heat transfer and to visualise the time-dependent thermal distribution. In the following, we will study two cases; the thermal distribution along one LED and between two LEDs connected in series with different separation distance, d.

2.2.1 One LED

Numerically speaking, Eq. 4 can be simplified further by making it dimensionless. If we let $\bar{x} = x/L$, $\bar{T} = (T - T_2)(T - T_1)$, and $\bar{t} = t\alpha/L^2$ [23], then Eq. 4 can be written as

$$\frac{\partial \bar{T}(\bar{x}, \bar{t})}{\partial \bar{t}} = \frac{\partial^2 \bar{T}(\bar{x}, \bar{t})}{\partial \bar{x}^2} \quad (6)$$

Therefore, Eq. 5 becomes

$$\left.\frac{\partial \bar{T}}{\partial \bar{x}}\right|_{\bar{x}=0} = 0$$
$$\bar{T}(\bar{x} = 0, \bar{t}) = \bar{T}(\bar{x} = 1, \bar{t}) = 0 = T_1 = T_{\text{room}} \quad (7)$$
$$\bar{T}_0(\bar{x}, \bar{t} = 0) = 1 = T_2 = T_{\max}$$

The essence of all numerical schemes for solving differential equations lies in the discretisation of the continuous variables, that is, the spatial coordinates and time [49]. A conventional numerical approach to the solution of the heat transfer equation is the finite difference discretisation method (FDDM). This scheme is almost standard in numerical methods that are based on computational grids as it is considered an important and one of the simplest forms of discretisation [50]. FDDM has been used extensively in numerical thermal analysis for numerous thermal systems [51,52,53,54,55]. With this method, the dimensionless time parameter $\bar{t}$ is divided into $n_{\bar{t}}$ discrete time points $\bar{t}_k = \bar{t}_0 + k\,\Delta\bar{t}$, with $k = 0,1,2 \ldots, n_{\bar{t}} - 1$, where $\bar{t}_{min} = \bar{t}_0$ and $\bar{t}_{max} = \bar{t}_{n_t}$. In this way, the time the interval $[\bar{t}_{min}, \bar{t}_{max}]$ is divided into $n_{\bar{t}}$ subintervals of size $\Delta\bar{t}$, where $\Delta\bar{t} = \frac{\bar{t}_{max} - \bar{t}_{min}}{n_{\bar{t}}}$. The same can be applied on the dimensionless spatial variable where $\bar{x}$ is divided into $n_{\bar{x}}$ discrete and equally spaced mesh points $\bar{x}_i = \bar{x}_0 + i\,\Delta\bar{x}$, with $i = 0,1,2,\ldots, n_{\bar{x}} - 1$, $\bar{x}_{min} = \bar{x}_0$ and $\bar{x}_{max} = \bar{x}_{n_{\bar{x}}}$ with a spatial step of , $\Delta\bar{x} = \frac{\bar{x}_{max} - \bar{x}_{min}}{n_{\bar{x}}}$. The initial state of the system is chosen to be the source solution which is given by:

$$\bar{T}_0(\bar{x}, \bar{t} = 0) = A \exp\left(-\frac{(\bar{x} - \mu)^2}{4\sigma}\right) \quad (8)$$

Where A, μ, σ are the height, centre and width of the initial state, respectively. Figure 2-a shows the temperature distribution along the LED for different time steps. It can be seen that at $\bar{t} = 0$ the temperature distribution has a shape of a squared (step) function where it has a constant value of $\bar{T}(\bar{x}, \bar{t} = 0) = 1$ for any spatial value $\bar{x}$ apart from the boundary points $\bar{x} = -L/2$ and $\bar{x} = L/2$ where $\bar{T}(\bar{x} = \pm L/2, \bar{t}) = 0$ which matches the boundary conditions. As the time goes by, i.e., $t > 0$, it is clearly noticeable that the temperature distribution is dissipated, and its height decreases which means that the LED's temperature is becoming lower with time. Figure 2-b. shows that the centre of the LED, in the blue line, cools slower than points near the ends, in the red line. However, the green line refers to the temperature at the boundary points where we can see that they maintain their room temperature throughout the process.

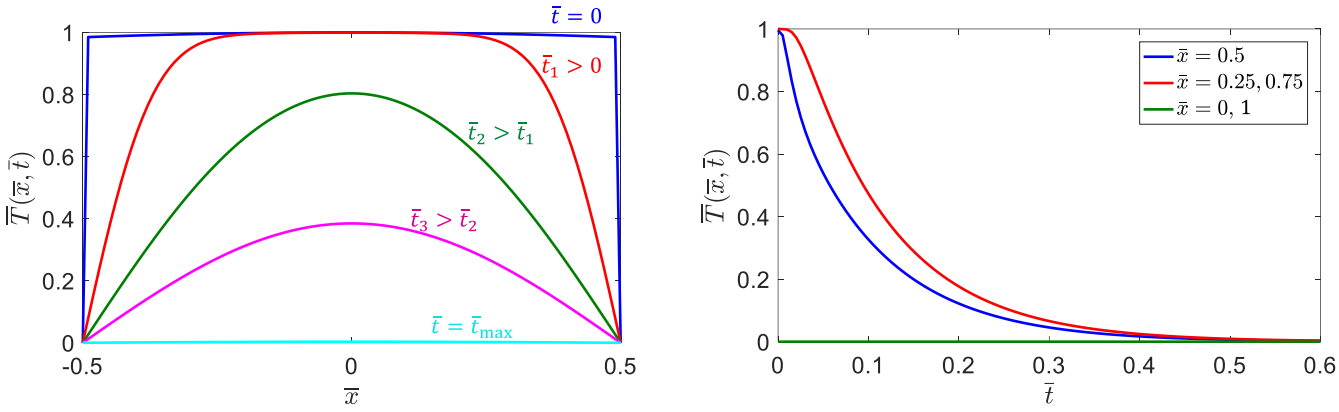

(a) (b)

Figure 2: The time-dependent temperature distribution $\bar{T}(\bar{x},\bar{t})$ along one LED with a length L. (internal temperature distribution); (a) shows $\bar{T}(\bar{x},\bar{t})$ as a function of the spatial variable $\bar{x}$ for different time steps and (b) illustrates the temperature distribution behaviour as a function of time for different LED positions: $\bar{x}=0.5$ (blue line), $\bar{x}=0.25{,}0.75$ (red line) and $\bar{x}=0, L$ (the green line). Here we have used: $A=1, \mu=0$ and $\sigma=4$ and $\bar{t}_{max}=0.6$.

It is worth mentioning that as Figure 2 describes, the cooling (temperature dissipation) process of the exact electronic device starting from $\bar{t}=0$ until $\bar{t}=\bar{t}_{max}$, this behaviour mirrors the heating process as it is considered as a reversed process to the cooling process. This simulation is related to the component itself.

2.2.2 Two LEDs connected in series with different separation *d*

Here, we assume two LEDs connected in series with a specific separation distance d between them. Both LEDs have the same length L and similar analysis as before will be done for them. The heat transfer equations and the initial states for both LEDs can be written as:

$$\frac{\partial \bar{T}_1(\bar{x},\bar{t})}{\partial \bar{t}}=\frac{\partial^2 \bar{T}_1(\bar{x},\bar{t})}{\partial \bar{x}^2} \qquad \bar{T}_0^1(\bar{x},\bar{t}=0)=A_1\exp\left(-\frac{(\bar{x}-\mu_1)^2}{4\sigma_1}\right) \qquad (9-\text{a})$$

$$\frac{\partial \bar{T}_2(\bar{x},\bar{t})}{\partial \bar{t}}=\frac{\partial^2 T_2(\bar{x},\bar{t})}{\partial \bar{x}^2} \qquad \bar{T}_0^2(\bar{x},\bar{t}=0)=A_2\exp\left(-\frac{(\bar{x}-\mu_2)^2}{4\sigma_2}\right) \qquad (9-\text{b})$$

Where $A_{1,2}, \mu_{1,2}, \sigma_{1,2}$ are the heights, centres and widths of the initial states of the left $\bar{T}_0^1(\bar{x},\bar{t}=0)$ and right $\bar{T}_0^2(\bar{x},\bar{t}=0)$ LED respectively. $\bar{T}_1(\bar{x},\bar{t})$ and $\bar{T}_2(\bar{x},\bar{t})$ are the solutions for left and right LEDs. If $\bar{T}_{Total}(\bar{x},\bar{t})$ is defined as the total solution of the system, then it can be formulated as:

$$\bar{T}_{\text{Total}}(\bar{x},\bar{t})=\bar{T}_1(\bar{x},\bar{t})+\bar{T}_2(\bar{x},\bar{t}) \qquad (10)$$

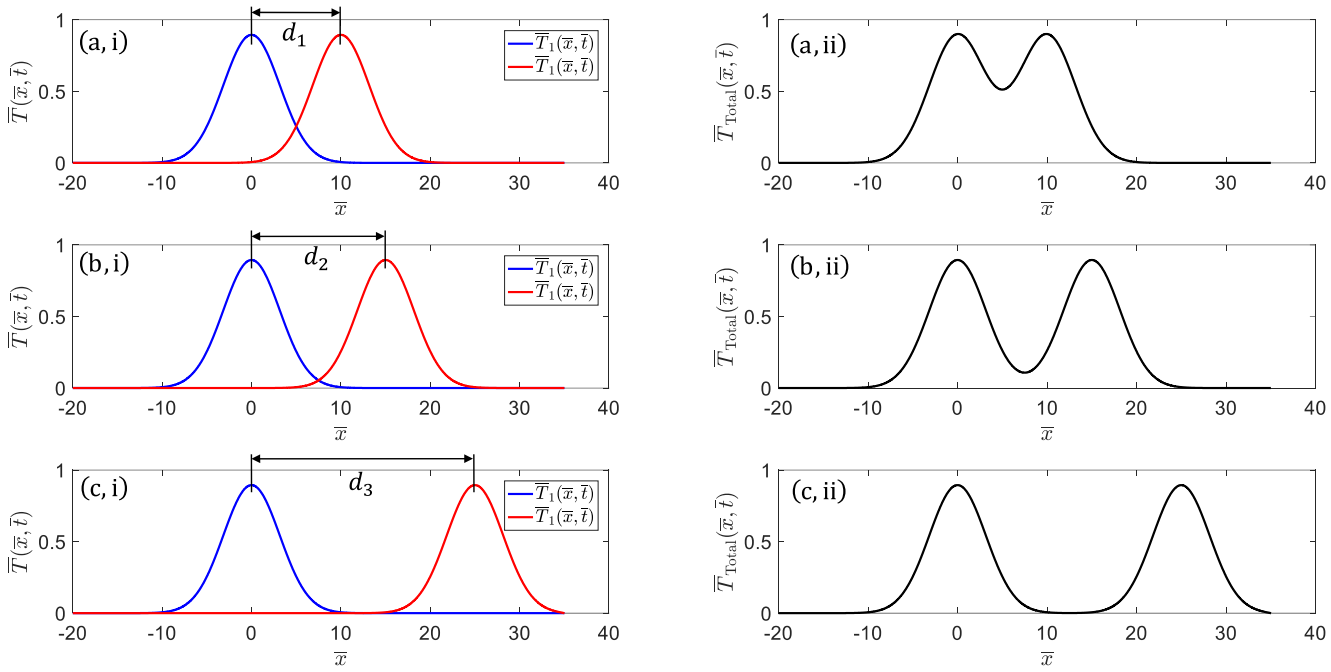

Figure 3: The oversimplified solutions of the one-dimensional and time-dependent partial differential equations for two independent LEDs expressed in Eqs. 9 at $\bar{t} = \bar{t}_{\max}/2$, where the blue line represents the left LED, i.e., $\bar{T}_1(\bar{x},\bar{t})$, and the red line represents the right one, i.e., $\bar{T}_2(\bar{x},\bar{t})$ in (a, i), (b, i) and (c, i) for different separations with $d_1 < d_2 < d_3$. However, (a, ii), (b, ii) and (c, ii) show the total thermal distribution, i.e., $\bar{T}_{Total}(\bar{x},\bar{t})$, for the system of two LEDs. Here we have used $A_1 = A_2 = 1, \mu_1 = 0, \mu_2 = 10, 15, 25, \sigma_1 = \sigma_2 = 4$ and $\bar{t}_{max} = 2$.

Figure 3 shows that for small separation values d between both LEDs, the total thermal distribution tends to overlap as a result of the summation between $\bar{T}_1(\bar{x},\bar{t})$ and $\bar{T}_2(\bar{x},\bar{t})$, as in Figure 3-a, ii. However, for a large separation, the total thermal distribution acts as two separate distributions. This means that for large separations the thermal effect between both LEDs is minimal as if they do not effect each other, as shown in Figure 3-c, ii. This, however, does not reflect the real system. In reality, the total thermal profile is not just the summation of each LED's thermal distribution; there is actually a thermal effect from each LED on the other leading to a higher and wider thermal profile. Therefore, the left and right solutions, $\bar{T}_1(\bar{x},\bar{t})$ and $\bar{T}_2(\bar{x},\bar{t})$, need to be modified in order for the total $\bar{T}_{Total}(\bar{x},\bar{t})$ in Eq. 10 to be accurate and to demonstrate the actual behaviour. For that matter, we formulate the new total thermal distribution formula as following:

$$\psi_{\text{Total}}(\bar{x},\bar{t}) = \xi\left(\psi_1(\bar{x},\bar{t}) + \psi_2(\bar{x},\bar{t})\right) \tag{11}$$

where we have assumed:

$$\psi_{1,2}(\bar{x},\bar{t}) = \bar{T}_{1,2}^{`}(\bar{x},\bar{t}) + \lambda_{3,4}\bar{T}_{2,1}^{`}(\bar{x},\bar{t}) \quad \begin{cases} \bar{T}_{1,2}^{`}(\bar{x},\bar{t}) = \lambda_{1,2} + \bar{T}_{1,2}(\bar{x},\bar{t}) \\ \lambda_{1,2} = h_{1,2}\exp\left[-\dfrac{\left(x-\gamma_{1,2}\right)^2}{2s_{1,2}^2}\right] \\ \lambda_{3,4} = \exp\left[-\dfrac{x - x_{\max,\min}}{x_{\min,\max} - x_{\max,\min}}\right] \\ \xi = \dfrac{2}{3}\left[\max\left(\bar{T}_{1,2}(\bar{x},\bar{t})\right) + \dfrac{1}{\mu_2 - \mu_1}\right] \end{cases} \tag{12}$$

Where: $\bar{T}_{1,2}^{`}(\bar{x},\bar{t})$ are the modified left and right LED thermal distributions in the 2-LED system, ξ is the modulation coefficient, $\lambda_{1,2,3,4}$ are the correction functions, and $\gamma_{1,2}, h_{1,2}, s_{1,2}$ are $\lambda_{1,2}$ parameters. It can be seen from Figure 4 that the total thermal distribution, i.e., $\psi_{\text{Total}}(\bar{x},\bar{t})$ in the green solid line, illustrates the

mutual effect that each LED has on the other as its area under the curve is wider and higher comparing to each individual LEDs' thermal distributions, i.e., $\overline{T}_1(\bar{x},\bar{t})$ and $\overline{T}_2(\bar{x},\bar{t})$. It can be seen that for small distances, the simulation shows a complete overlap between both individual distributions. As the separation distance increases, the total thermal distribution starts to split into two peaks with maintaining its feature of being higher and wider than the individual distributions. It is worth noting here that the behaviour of the total thermal distribution $\psi_{\text{Total}}(\bar{x},\bar{t})$ can be simulated for a wide range of separation distances by changing the value of the difference between both LEDs' centres $\mu_2 - \mu_1$. This would allow us to theoretically estimate the optimal separation distance between both LEDs. For very large distances, the total thermal distribution tends to show the behaviour of individual thermal distributions as the LEDs cannot affect each other anymore.

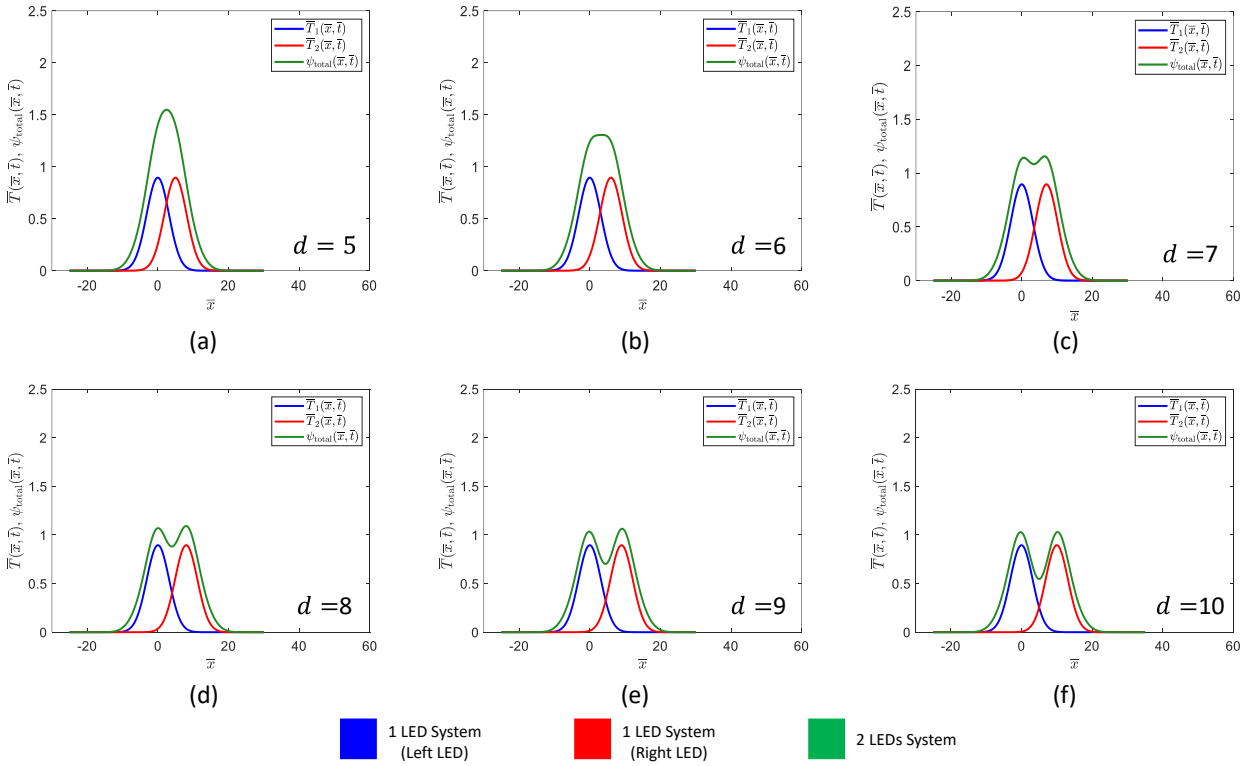

Figure 4: The total thermal distribution of a two-LED system with mutual effect for different separation values d at $\bar{t} = \bar{t}_{\max}/2$. The blue line represents the left LED, i.e., $\overline{T}_1(\bar{x},\bar{t})$, the red line represents the right one, i.e., $\overline{T}_2(\bar{x},\bar{t})$, and the green line refers to Eq. 11 where the total thermal distribution $\psi_{\text{Total}}(\bar{x},\bar{t})$ is the sum of the modified solutions for each LED. Here we have used: for the corrected Gaussian function, $\gamma_1 = -5, \gamma_2 = 10\ (a), 11(b), 12(c), 13(d), 14(e), 15(f)$, $s_{1,2} = 3$, $h_{1,2} = \frac{1}{s_{1,2}\sqrt{2\pi}} = 0.13$, and for the initial source solutions $A_{1,2} = 1, \mu_1 = 0$, $\mu_2 = 5(a), 6(b), 7(c), 8(d), 9(e), 10(f)$, $\sigma_{1,2} = 4$ and $\bar{t}_{\max} = 2$.

3. Experimental Work

3.1 Overview

Any electronic device produces waste heat that leads to elevating its temperature; hence affecting its functionality, reliability and sustainability. Therefore, the need to manage, control and monitor a device's temperature and its thermal behaviour is becoming critical to enhance its performance and reliability. Infrared thermography is one of the ideal non-contact thermal evaluation tools that has been utilised in thermal management of electronics for some time [56, 57]. Infrared thermography can provide a 2D thermal image of electronic devices with an acceptable temperature measurement error. In this work, infrared camera type FLIR A310 is utilised with a special micro close-up 4x lens to take close-up infrared thermographic images of the LED samples with specifications of field of view (FOV) of 32mm x 24mm at 79mm distance. And Instantaneous Field of View (IFOV) or Spatial Resolution of 100µm (nominal) which is adjustable within a narrow range; and the used spatial resolution was circa 75µm. Additionally, a point-measurement technique

using a thermocouple is utilised, to ensure that accurate temperature measurements are recorded for calibration. Thermocouples can be placed in direct contact with areas to be measured, so that any measurement inaccuracy can be compensated. This also helps in the calibration process, in order to reach the sample's most accurate temperature. It is worth mentioning that all experimental work has been done inside a small environmental chamber so that any sudden temperature change in the surrounding environment will be minimal. Additionally, all the samples are matt-black painted to make the emissivity value of the system closer to the emissivity of a blackbody; it is estimated that the matt-black will reduce reflection and allow emissivity value to reach circa 0.98). The paint would add a thin layer of material, which may cause a slight delay in the thermal response seen by the infrared camera but it is not expected to significantly increase the temperature in steady state situation. And since the paint was applied in all scenarios, comparative or relative difference should be accurate. The paint should not also effect in terms of thermal distribution patterns. Basically, the experimental work starts with only one LED in the circuit, and then we add another one with different separations d between them to observe the resulting thermal effect of adding another LED to the circuit.

3.2 Samples Description

The LED samples used in this project are of dimensions 1.0x0.5x0.8mm and type SMD CHIP LAMP, with all LED features and specifications can be found in reference [58], which includes the manufacturer's data sheet. Figure 5 shows visual photos of a bare LED from three directions, front (Figure 5-a), back (Figure 5-b) and side (Figure 5-c), using a digital microscope. Figure 5-d shows the infrared camera with the LED in the environmental chamber. Note that the LED in the photo was not painted matt black in order to create a clearer image for the paper. Figure 5-e presents the scale of the LED when compared with the tip of a standard ball point pen.

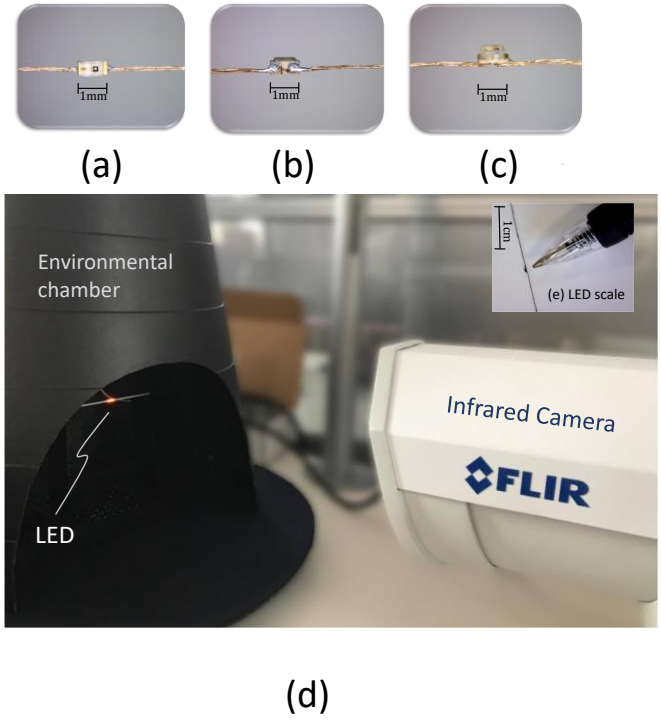

Figure 5: Illustration of a bare LED used in our project where (a) shows the front, (b) the back and (c) the side views of the LED. The pictures were taken using a digital microscope: Dino-Lite AM-311S; the experimental work setup (d), the scale of LED in comparison to a standard ballpoint pen (biro) (e).

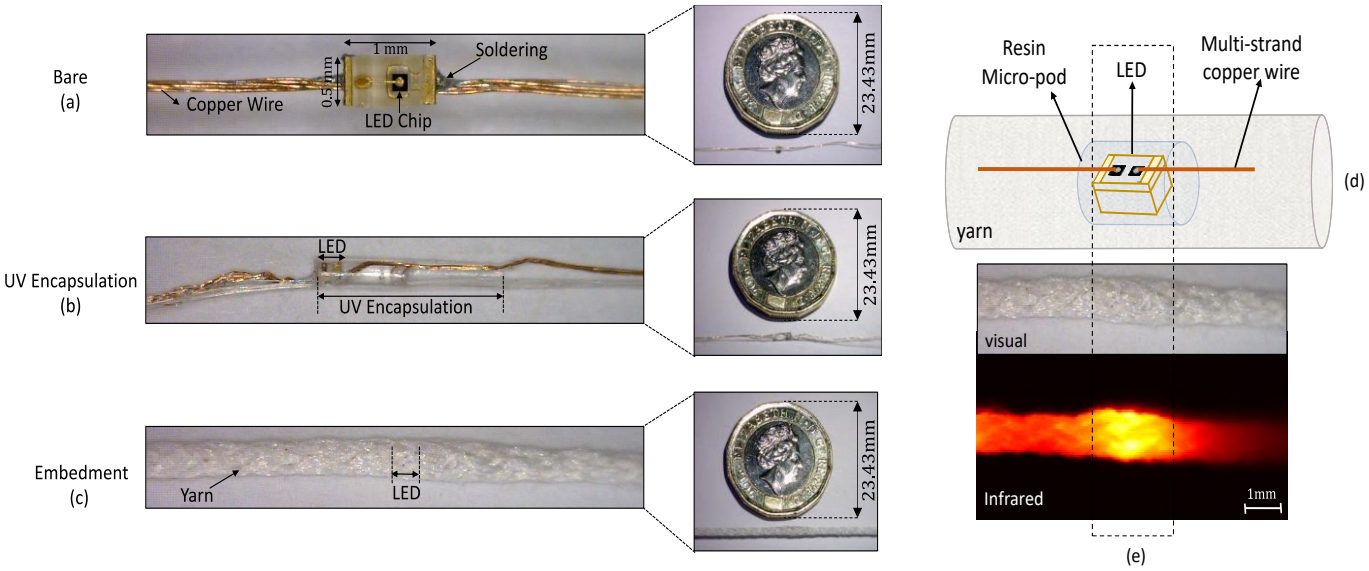

Figure 6: Three basic states of LED followed in smart textiles technology. (a) is the bare LED and its dimensions, (b) the encapsulated LED and (c) the embedded LED inside the yarn, (d) a sketch that clarifies the structure of the final textile, and (e) shows the visual and infrared version of the final yarn.

The production of an e-yarn, see Figure 6, consists of four main steps [59]:

- Firstly, the LED is soldered onto a fine copper wire, as shown in Figure 5 and Figure 6-a.
- As a protection procedure before integrating the device inside the yarn, the LED and the interconnects are then encapsulated using ultraviolet (UV) curable polymer resin to form a cylindrical micro-pod [60], as shown in Figure 6-b. The purpose of the encapsulation is to hermetically seal and protect the electrical components from environmental effects, such as humidity and dust, which means that the resulting e-yarn could be washed. Other benefits include improving electrical insulation, reliability, robustness, and protection against damage of the e-yarn in the final product [61]. In this work, a photo-initiated curing method, i.e., an ultraviolet curable coating, is chosen for the encapsulation process. This is due to low operational cost, easy maintenance, and the small footprint of space required for machinery. A UV-curable system is normally composed of three basic components:
    1. A resin, which is an unsaturated double bond or cyclic structure capable of ring opening. Commercially available UV curable resins can be categorised by the polymerization mechanisms through which curing takes place. An acrylated urethane is chosen for this research: Dymax 9001-E-V3.5 (Dymax, Torrington, UK). This is transparent to visible light, making it suitable for encapsulation of LEDs. Moreover, this resin is flexible, so it is suitable for textile applications. The resin is also used in bonding applications in the electronics industry, meaning that it has been fully tested on a range of electronic devices [62].
    2. Reactive diluents, which have two functions: to reduce the viscosity of the systems and to render crosslinking.
    3. A photo-initiator, which absorbs UV radiation and generates reactive species that can initiate the polymerisation.

    Resin micro-pods can be formed by applying a small amount of resin around the LED or by placing the LED (soldered to copper wire) within a mould, then injecting the resin into the mould. The latter method is chosen in this work to ensure uniformity of the micro-pod size. A cylindrical micro-pod shape is chosen for encapsulating the soldered LED, as this shape has minimal edges. This shape is also easier to pass through the small-diameter wrap-knitting machine that is used in a later stage of the e-yarn production, not to mention that it is more likely to be user-friendly.

The final two stages involve the addition of textile yarns twisted around the copper wire. Three cotton yarns (NM 30/1*2 Davidoff; Boyar Textile, Istanbul, Turkey) were twisted around the copper wire [63] using an Agteks DirecTwist 2B6 machine (Agteks, Istanbul, Turkey) at 10 m min^{-1} [64].

3.3 Thermal profile of one LED

For the case of one LED, a current of $I = 0.02$ A and voltage of $V = 2$ V are applied on the circuit for all experiments. Figure 7 shows the calibrated 2D infrared images for one LED in its bare condition (a), encapsulated in (b), and embedded state in (c) and their corresponding thermal distributions. Linear-interpolation method is implemented to calibrate the infrared temperatures taken from the thermal images using the thermocouple temperature readings. It can be seen in Figure 7 that the average temperature of the LED is about 34^0C. This temperature decreases noticeably in embedded state where the LED's temperature reaches 27.5^0C, due to the increase in material around the LED and the heat dissipation process. For the bare LED, the heat dissipation occurs by convection to the surrounding air and by conduction to the copper wires. For the bare LED it has also been noticed that the infrared image readings are sensitive to the orientation (angle) of the LED relative to the camera, this will be discussed further in the following sections. Please note that the axis is a direct presentation of the location of the infrared image pixels; and hence it is labelled in that way.

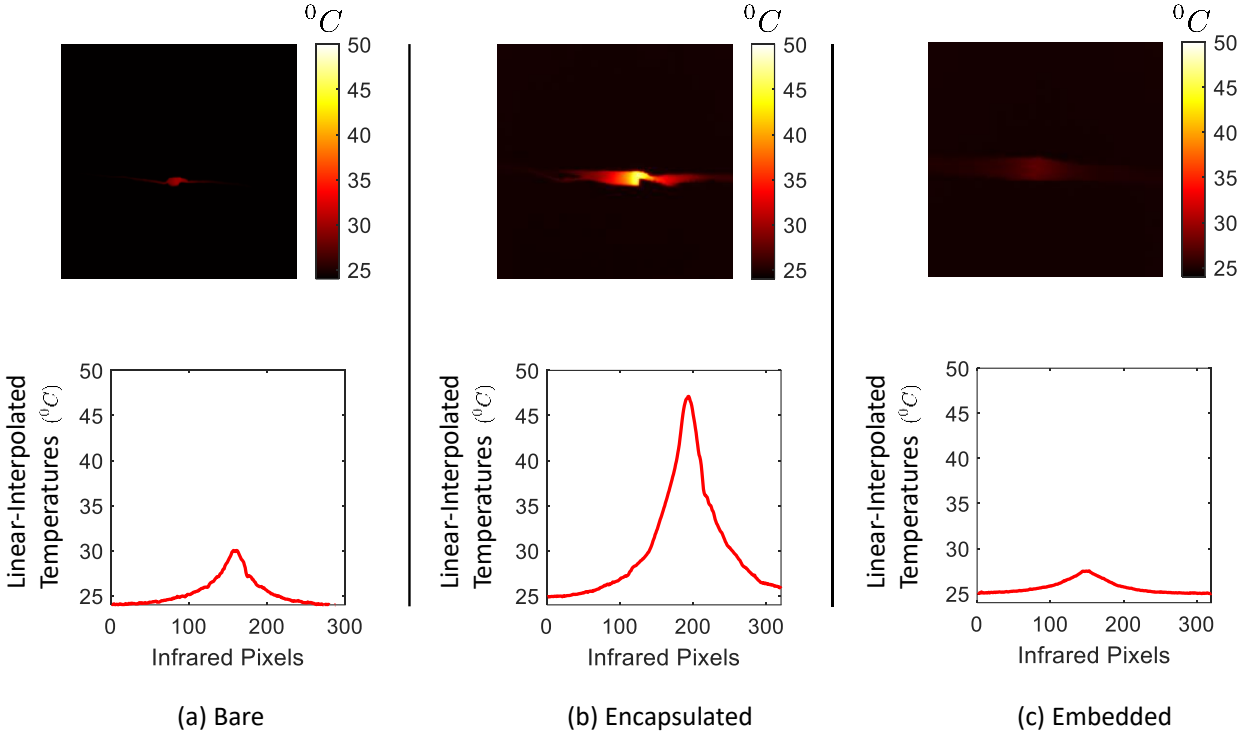

Figure 7: Linear-interpolated 2D images created by MATLAB for one LED and its corresponding thermal distribution plots based on the temperatures taken from a directly touched thermocouple to a bare (a), encapsulated (b) and embedded (c) LED. All temperatures are in ^0C.

3.4 Thermal profile of two LEDs

Here, we add one additional LED to the circuit with a distance d between both LEDs and apply a current of $I = 0.02$ Amp and a voltage of $V = 4$ volts on the circuit for all experiments. For different values of d, Figures 8, 9 ,10 show three infrared images each taken to two bare, encapsulated and yarn embedded LEDs for $d = 5$mm (a), $d = 10$mm in (b) and $d = 20$mm in (c), respectively, with their corresponding thermal distribution plots.

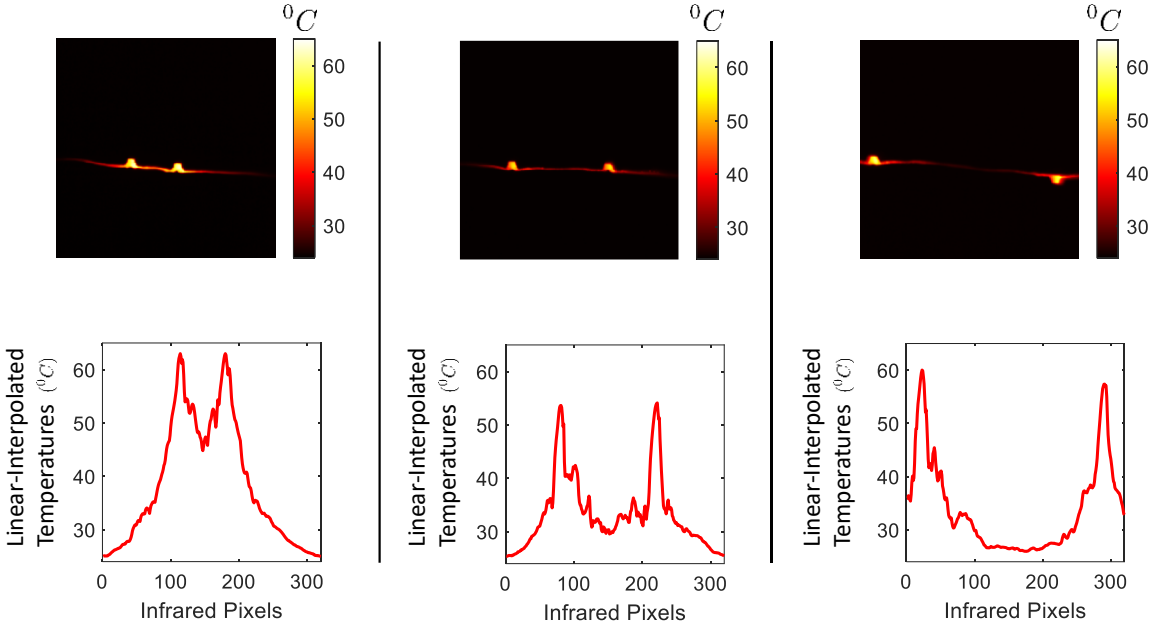

(a) $d = 5\text{mm}$ (b) $d = 10\text{mm}$ (c) $d = 20\text{mm}$

Figure 8: Bare LEDs. Linear-interpolated 2D images created by MATLAB for two *bare* LEDs and their corresponding thermal distribution plots; with separation distance (d) between both LEDs of $d = 5\text{mm}$ in (a), $d = 10\text{mm}$ in (b) and $d = 20\text{mm}$ in (c).

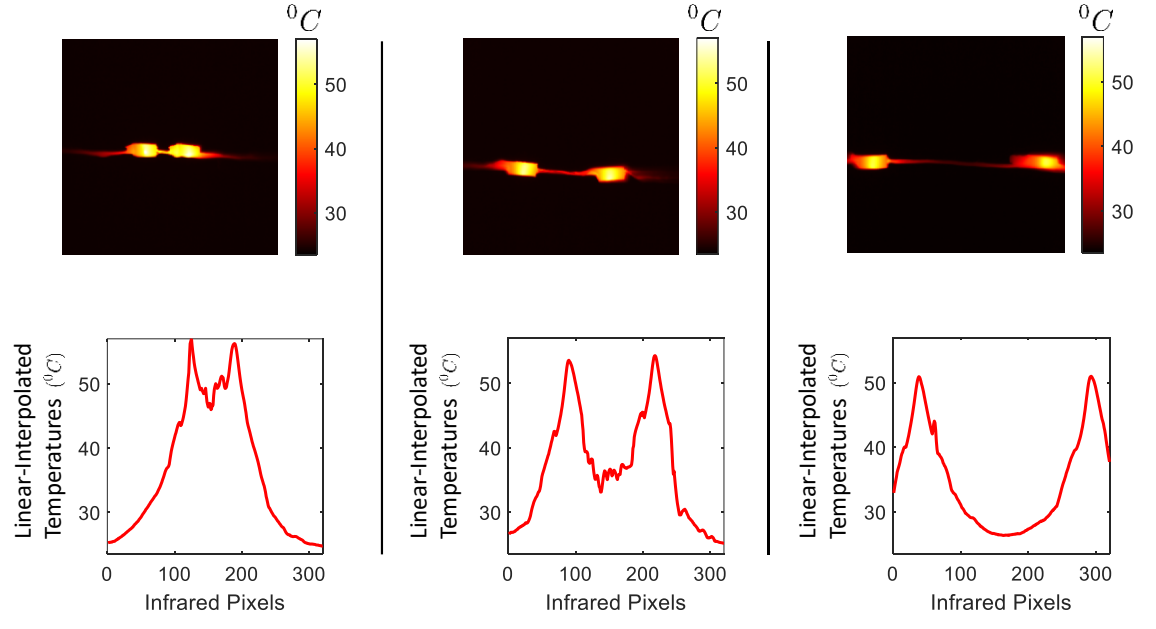

(a) $d = 5\text{mm}$ (b) $d = 10\text{mm}$ (c) $d = 20\text{mm}$

Figure 9: Encapsulated LEDs. Linear-interpolated 2D images created by MATLAB for two *encapsulated* LEDs and their corresponding thermal distribution plots; with separation distance (d) between both LEDs of $d = 5\text{mm}$ in (a), $d = 10\text{mm}$ in (b) and $d = 20\text{mm}$ in (c).

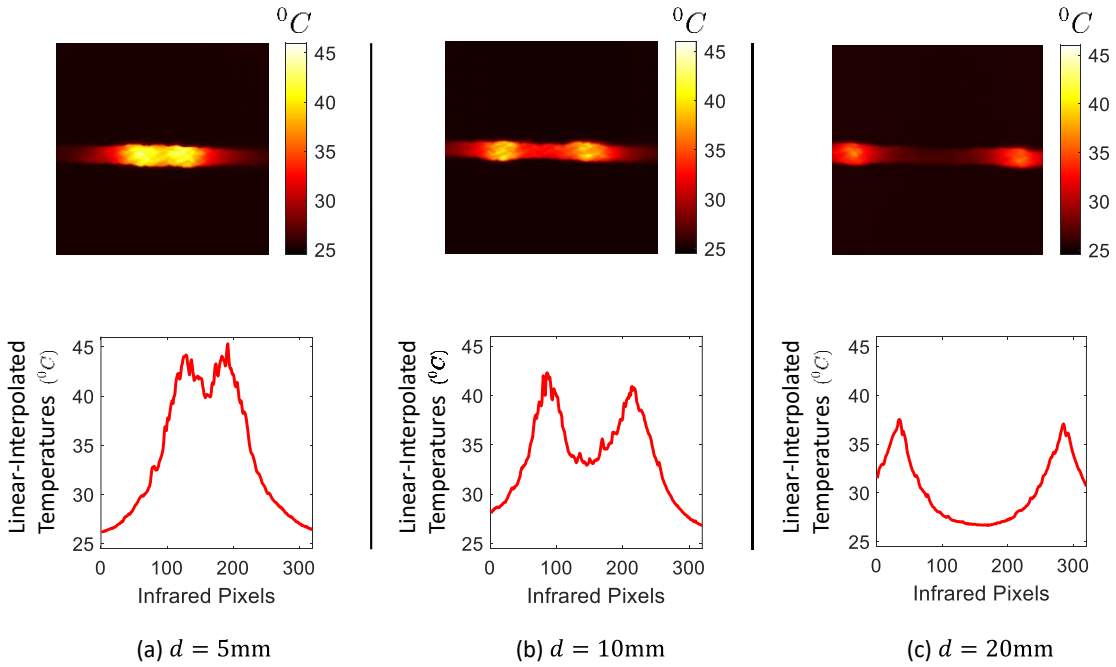

Figure 10: Yarn embedded LEDs as (described in section 3.2). Linear-interpolated 2D images created by MATLAB for two *embedded* LEDs and their corresponding thermal distribution plots; with the separation between both LEDs is $d = 5$mm in (a), $d = 10$mm in (b) and $d = 20$mm in (c). All temperatures are in ^0C.

It can be easily noticed from the above plots that the thermal distribution maintains its Gaussian-like shape even after adding an additional LED to the circuit. Moreover, the system temperature is inversely proportional to the separation between both LEDs as d increases the system's temperature decreases accordingly. Similar to the one LED case, the temperature of two embedded LEDs is lower comparing to the encapsulated and bare states.

3.5 Two-dimensional knitted garment

In this sub-section, we study the two-dimensional (2D) thermal distribution of one and two LEDs with a specific distance d embedded in knitted garment. The garment is knitted from the same textile yarns twisted around the copper wire using three cotton yarns as discussed in section 3.2 above. Knitted fabric is a textile that results from knitting, the process of inter-looping of yarns or inter-meshing of loops. Because of its flexibility, it can be constructed into different smaller pieces, making it ideal for wearable garments and other applications. In this work, rectangular knitted samples (circa 10cm x 12cm) were produced on a computerized flat-bed knitting machine using an intarsia knitting technique; and the fabric was created using cotton yarns. The aim here is to analyse the 2D thermal distribution in the garment and to estimate the proper distance between two LEDs in the garment based on their thermal distribution. Figure 11 shows the 2D knitted Garment used in this project.

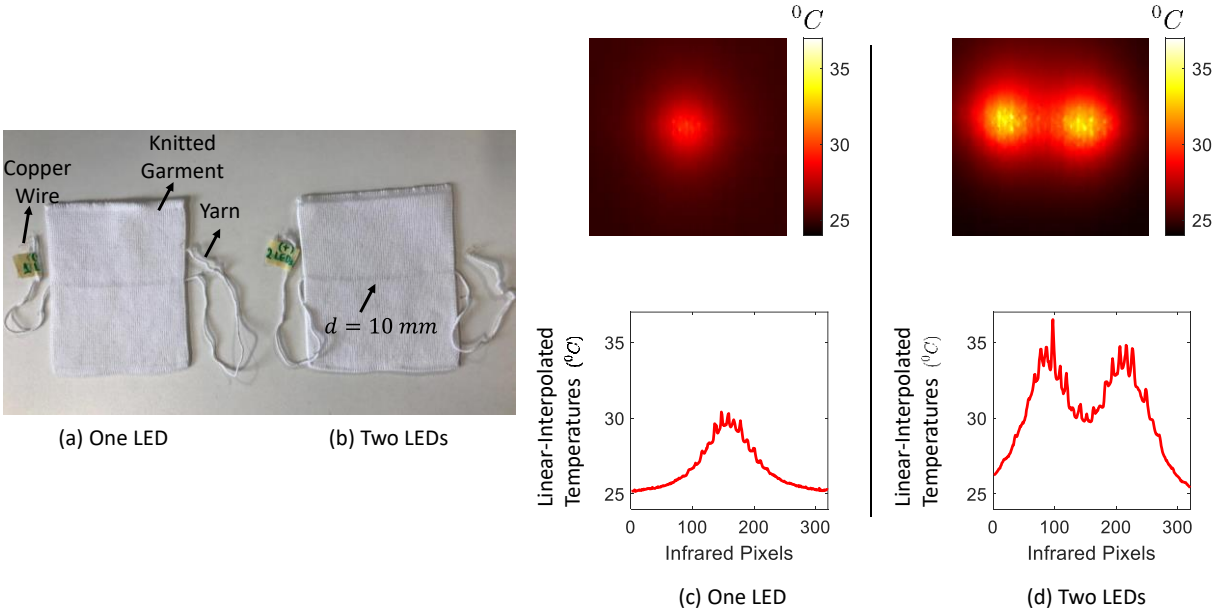

Figure 11: 2D knitted garments with one LED in (a) and two LEDs in (b) with a distance $d = 10$ mm between both of them. 2D MATLAB generated images of the 2D knitted garments with the corresponding linear-interpolated thermal distribution plots are in (c) and (d). All temperatures are in ^0C.

Figure 11 shows the 2D infrared calibrated images for the 2D samples and their corresponding thermal distribution plots. We notice that the 2D thermal distribution has a similar Gaussian-like shape as before in case of one and two LEDs. Additionally, we have seen earlier that when the distance between two LEDs is $d = 5$ mm then the total thermal distribution is highly overlapping and the thermal effect of each LED on the other is greatly noticeable. However, when the distance is $d = 20$ mm, the thermal effect of both devices at each other is at its minimal value. In our experiment here, we have chosen the distance to be $d = 10$ mm and it is clearly observed from Figure 11-d that the thermal distribution of both LEDs is neither greatly overlapping nor distantly separated. Therefore, we can estimate the optimal distance between both LEDs to be in the range of $10 \leq d \leq 20$ mm so the thermal effects would be acceptable.

4. Discussion

In this research work, we have studied numerically by solving the heat transfer equation and experimentally by using infrared thermography the thermal distribution of heat caused by LEDs as bare, encapsulated and yarn embedded electronic devices in smart textiles. Various important points should be mentioned and discussed as results of this work:

4.1 Thermal profile

The experimental results have shown that the LEDs dissipate relatively significant amount of heat with Gaussian-like profile. This have been also illustrated numerically as the solutions of the heat transfer equation own a similar shape. It is worth mentioning that this shape does not change in case of adding another LED to the circuit or by changing the value of the system's emissivity, but overlap would occur depending on the distance with different temperature gradient. Parameters that influence the absolute temperature profile, given that any other parameters are fixed, include the distance between the two LEDs and their mutual effect, the encapsulation of the LEDs, the yarn around the encapsulated LEDs and the heat dissipation process in conduction through knitting of the garment. The relationship, however, is complex as thermal capacity and heat transfer process will be affected by each change in the encapsulation of the LEDs and the knitting process; and more work is needed in this area as will be described in the following sections.

4.2 Temperature difference as a function of distance between LEDs

As a part of this work, we have analysed the temperature behaviour of two LEDs connected in series in the textile's circuit. It has been clearly shown that not only the temperature of the two-LED system is noticeably higher than the one-LED system but also the distance between both LEDs has a crucial effect on the overall system's temperature. We have seen that the closer the LEDs, i.e., the smaller the distance, the higher the overall temperature. Statistically speaking, Figure 12-b shows the calibrated temperatures for the two LEDs at different distances, and it can be seen that their temperatures get lower with increasing the distance between them. Figure 12-c shows that the 2D garment that includes one LED produces a temperature that is lower comparing to the case of the two-LED system.

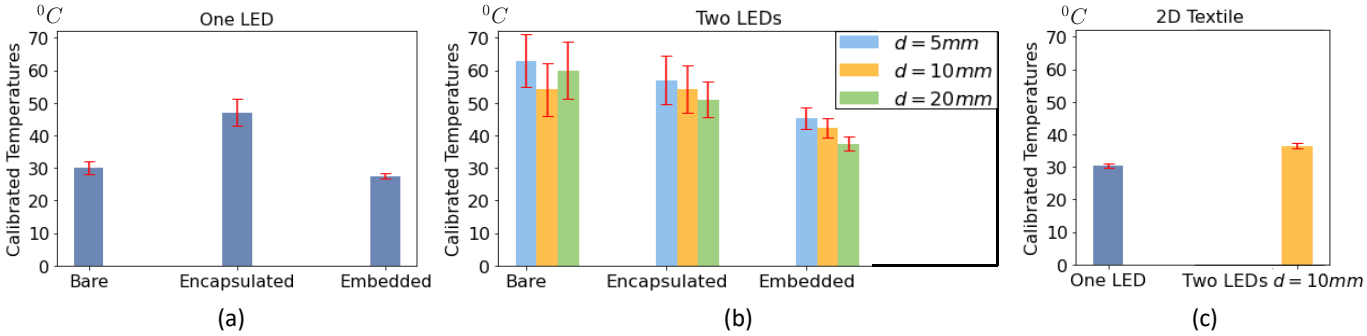

Figure 12: Bar charts of the linear-interpolated and calibrated temperatures for one LED in its three different states; bare, encapsulated and embedded n (a); for two LEDs with different distances (b); and for 2D knitted garments for one and two LEDs embedded inside the yarn (c).

It seems from the results that the cover yarn can help dissipating the heat, which could be related to increasing the heat transfer via conduction through the material and the increase in diameter, and hence the volume and external surface. This would also help in enhancing the thermal convection. Therefore, the selection of the material and structure is critical to the thermal performance of electronic devices embedded in e-textiles. This would explain the reason why the 2D knitted garment has a slightly lower temperatures.

4.3 Error Analysis

All the experimental temperature data are certainly associated with error that relates to many factors, such as environment temperature change, human error, etc. One of the key errors in the experimental work of bare LEDs is the orientation relative to the infrared camera. Due to the small size of the LEDs, the orientation has been found to be very critical to the measurement. This error is found not to be significant in relation to the encapsulated and embedded LEDs due to the heat dissipation by conduction. However, the infrared data has also variation and noise during the measurement process on pixel level along the length of the yarns. To assess this error, the collected data is compared with its moving average. The moving average method is chosen as it helps in reducing noise, determining the underlying trends, and removing random variations in the infrared data. The moving averages are a series of averages calculated using sequential segments of data points over a series of values; where 10 data points are chosen for this calculation. Using this, the average error E_{avg} and the standard deviation std, between the averaged and the infrared data points were calculated. It can be noticed that the averaged error (E_{avg}) is within a fraction of a degree as shown in Figure 13

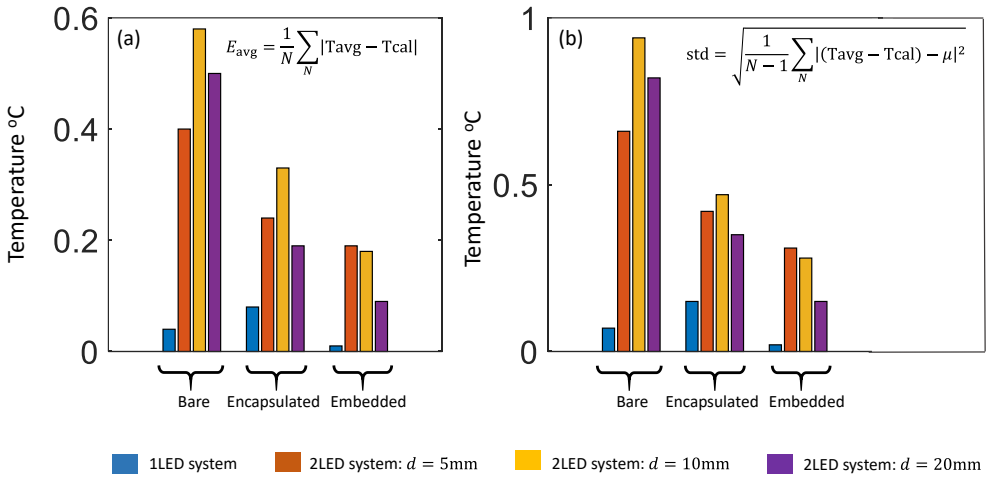

Figure 13: Error analysis between the experimental and averaged smoothed data for all textile stages in both systems: one-LED and two-LED. (a) the average error, E_{avg}; and (b) the standard deviation, std.

The same error analysis is carried out on the 2D textiles temperature data points, as shown in Figure 14. It can be noticed here that the averaged error (E_{avg}) and the standard deviation (std) are both approximately within 0.3 of a degree centigrade.

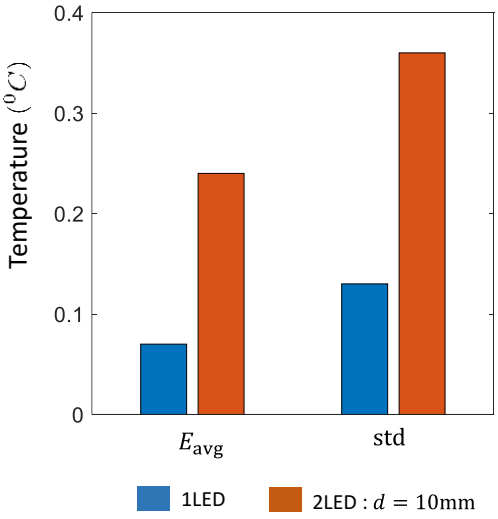

Figure 14: Error analysis between the experimental and averaged smoothed data for 2D textiles for one-LED and two-LED systems with a separation distance of $d = 10$mm.

4.4 The accuracy between the theoretical and experimental data

It is tempting to draw a comparison between the experimental and the theoretical results to examine the core differences between them. Figure 15 shows that there is a clear resemblance between both outcomes where it is obvious that the actual total thermal distribution of both LEDs is higher and wider comparing with the summation of both distributions that refer to individual LEDs. This has been shown experimentally and also has been analysed mathematically; so the resultant profile reflects an accurate thermal phenomenon.

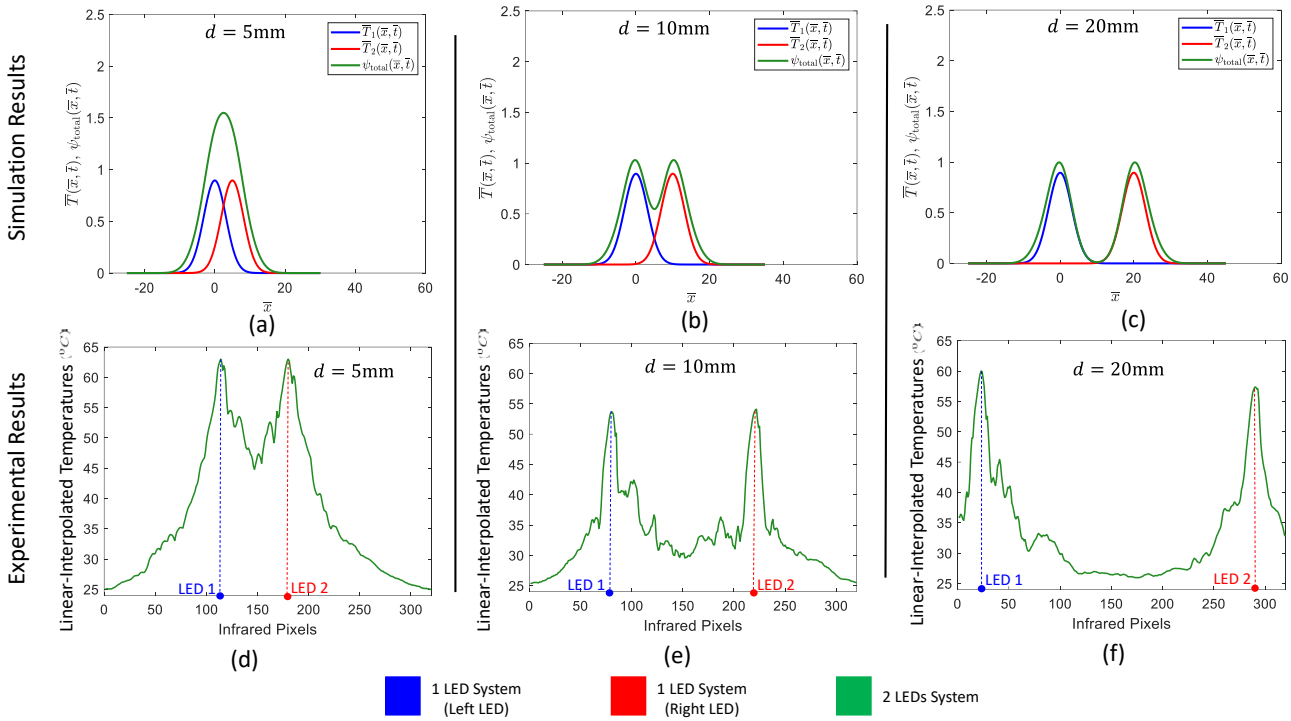

Figure 15: The relationship between the separation distance between the two bare LEDs and the overall system temperature. Sub-figures (a), (b) and (c) show the mathematical simulation; while sub-figures (d), (e) and (f) show the experimental results. The green solid line represents the two-LED system and the blue and red lines represent the one-LED system.

To reduce errors and variation in experimental infrared data, the following aspects should be taken into consideration when using infrared thermography to conduct similar work:

- Emissivity of the system should be taken into consideration.
- The distance between the camera and the sample should be fixed to simplify the calibration process and comparison between the tests.
- The voltage and the current values should be monitored or controlled during the experiments.
- Taking the temperature measurement when steady state is reached.
- The experiment must be carried out in stable environmental conditions.

4.5 Optimal distance between two LEDs

We have seen so far that the total or resultant thermal distribution tends to highly overlap for small distances, i.e., $d = 5$ mm, and acts as two separate thermal distributions for large distances, i.e., $d \geq 20$ mm. Since thermal overlapping leads to a high temperature outcome, small separation distances would create higher temperature levels. However, as the separation distance increases, the produced temperatures become within the acceptable thermal range and the final design would be more practical for long term reliability. Figure 16 presents the interpolation of the temperature produced from the two-LED system at any given distance within the range of $5 \leq d \leq 20$ mm. This certainly helps to better understand the multi-LED system with separation distances different from the ones proposed in this work.

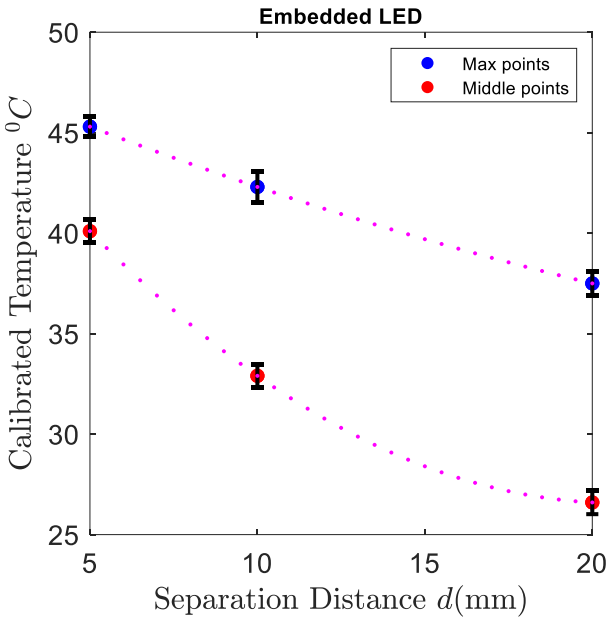

Figure 16: The behaviour of the max (blue circles) and middle (red circles) points of Two-LED systems' thermal distributions as a function of separation distance between the two LEDs, d(mm) for the embedded yarn.

All in all, we have seen that temperature is one of the most crucial characteristics that needs to be studied; and effective methods and ways to analyse its effects on the performance of electronic devices in e-textiles should be developed. In our work, numerical investigation has been conducted by solving the partial differential equation of the heat transfer to simulate the thermal distribution within the device. Infrared thermography as well as thermocouple thermal techniques have been also used effectively to measure and record the overall temperature of our system. Not only both results have been equivalent but also, we have identified various significant experimental elements that could lead to more reliable outcomes. The importance of this research work is to show the significance of the heat dissipated from LEDs and the effect of the distance between them on the overall temperature. Hence, for reliable systems in the future, two approaches will be needed: (1) the development of high efficiency LEDs of small size that could operate reliably at higher temperatures; and (2) in the meantime maintaining suitable distance between LEDs to avoid temperature increase due to lower thermal dissipation which could significantly reduce reliability on the long term. This distance will depend on many factors including environmental conditions, efficiency of LEDs and length of operation; and performance should be investigated for each design and operation scenario to ensure high reliability.

5. Conclusion and Future work

Temperature is one of the most crucial characteristics that needs to be studied to ensure high reliability of electronic textiles. The paper has presented a novel approach of using infrared thermography, with mathematical differential equations and numerical analysis, to investigate the thermal characterisation of embedded electronic devices in e-textiles. The results, theoretically and experimentally indicate the importance of the heat dissipation process that could be one of the limiting factors in developing high density sensory and actuation systems in smart textiles. LEDs have been used as the actuator to assess the heat dissipation; as with the very small size LEDs and combined with encapsulation for the smart textile, the temperature issues could become a limiting factor in the capabilities of the technology and hence heat dissipation is a critical factor to consider in any future design and operation, particularly if used on human body and in hot climates; where heat dissipation becomes a problem. An infrared camera is utilised with a micro close-up lens to capture infrared images of the LED samples, where infrared images are calibrated using a thermocouple contact measurement. The results of this work provide evidence that using infrared thermography can provide significant non-contact information about the thermal behaviour of smart textiles; and the same technique could be used in the future to evaluate e-textile products before introducing them to market. It has been found that the thermal distribution of the integrated LEDs has a Gaussian-like distribution which gets higher and wider by adding additional LEDs to the circuit within a specific distance range; this

plays a crucial role in determining the overall temperature of the system and shaping the final overall thermal distribution, and hence the potential thermal reliability of the smart textile on the long term. It s evident from the experimental data that the cover yarn in terms of material and structure could influence the thermal dissipation process. Future research should explore different heat dissipation design parameters to enhance reliability. The effect of yan and encapsulation materials on heat dissipation should be considered further in future work. Due to the small scale electronic components, we have found that more work is needed to fully understand the transient and steady state thermal behaviour of smart textiles.

6. Acknowledgements

This research was funded by the Engineering and Physical Sciences Research Council (EPSRC) under grant number EP/M015149/1 as a partnership project entitled "Thermal characterisation of embedded electronic devices in textile applications using infrared thermography". Special thanks is due to Professor Stephen Beeby at University of Southampton. We also would like to thank Professor Tilak Dias at Nottingham Trent University and his Advanced Textiles Research Group (ATRG), including Ioannis Anastasopoulos, M-Nour Nashed, Jose Carlos Oliveira and Dorothy Hardy for their great help in providing us with the LED samples that we have utilised for the experimental part of this project.

References

[1] Koncar, V., 2019, Smart textiles for monitoring and measurement applications, Editor(s): Vladan Koncar, In The Textile Institute Book Series, Smart Textiles for In Situ Monitoring of Composites, Woodhead Publishing, Pages 1-151, ISBN 9780081023082, https://doi.org/10.1016/B978-0-08-102308-2.00001-2.

[2] Paepegem, W. V., 2015, Fatigue testing and online inspection of carbon textile composites for aeronautical applications, Editor(s): Valter Carvelli, Stepan V. Lomov, In Woodhead Publishing Series in Composites Science and Engineering, Fatigue of Textile Composites, Woodhead Publishing, Pages 353-382, ISBN 9781782422815.

[3] Ritter, A., 2016, Smart coatings for textiles in architecture, Editor(s): Jinlian Hu, In Woodhead Publishing Series in Textiles, Active Coatings for Smart Textiles, Woodhead Publishing, Pages 429-453, ISBN 9780081002636, https://doi.org/10.1016/B978-0-08-100263-6.00018-6.

[4] Nauman, S., Lubineau, G., 2021, Chapter 4 - Nanocomposite sensors for smart textile composites, Editor(s): Andrea Ehrmann, Tuan Anh Nguyen, Phuong Nguyen Tri, In Micro and Nano Technologies, Nanosensors and Nanodevices for Smart Multifunctional Textiles, Elsevier, 2021, Pages 55-81, ISBN 9780128207772, https://doi.org/10.1016/B978-0-12-820777-2.00004-2.

[5] Jiang, C., Wang, K., Liu, Y, Zhang, C., 2021, Wang, B., Application of textile technology in tissue engineering: A review, Acta Biomaterialia, Volume 128, 2021, Pages 60-76, ISSN 1742-7061, https://doi.org/10.1016/j.actbio.2021.04.047.

[6] L. Berglin, "Smart Textiles and Wearable technology-A Study of Smart Textiles in Fashion and Clothing". The Swedish School of Textiles, 2013.

[7] A. Chinnappan, C. Baskar, S. Baskar, G. Ratheesh and S. Ramakrishna, "An Overview of Electronspun Nanofibers and Their Applications in Energy Storage, Sensors and Wearable/Flexible Electronics". J. Mater. Chem. C, 2017, Advance Article, DOI: 10.1039/C7TC03058D.

[8] K. Bogan, A.F.M. Seyam and J. Slade, "Evaluation of the Electrical Integrity of E-Textiles Subjected to Environmental Conditions". The Journal of The Textile Institute, 2017, DOI: 10.1080/00405000.2017.1350128.

[9] Y. Guo, K. Li, C. Hou, Y. Li, Q. Zhang and H. Wang, "Fluoroalkylsilane-modified Textile Based Personal Energy Management Device for Multifunctional Wearable Applications". ACS Appl. Mater. Interfaces 8 (2016) 4676–4683.

[10] H. Yu, X. Yang, Y. Lian, M. Wang, Y. Liu, Z. Li, Y. Jiang, and J. Gou, "An integrated flexible multifunctional wearable electronic device for personal health monitoring and thermal management". Sensors and Actuators A: Physical, volume 318, issue 112514, 2021.

[11] S. Li, Q. Zhong, J. Zhong, X. Cheng, B. Wang, B. Hu and J. Zhou, "Cloth-Based Power Shirt for Wearable Energy Harvesting and Clothes Ornamentation". ACS Appl. Mater. Interfaces 7 (2015) 14912–14916.

[12] Z. Gozutok, O. Agirbas, M. I. Bahtiyari, and A. T. Ozdemir, "*Low-voltage textile-based wearable heater systems fabricated by printing reactive silver inks*". Sensors and Actuators A: Physical, volume 322, issue 1123610, 2021.

[13] D. Son, J.H. Koo, J.K. Song, J. Kim, M. Lee, H.J. Shim, M. Park, M. Lee, J.H. Kim and D.- H. Kim, "*Stretchable Carbon Nanotube Charge-Trap Floating-Gate Memory and Logic Devices for Wearable Electronics*". ACS Nano 9 (2015) 5585–5593.

[14] M. Ha, J. Park, Y. Lee and H. Ko, "Triboelectric Generators and Sensors for Self-Powered Wearable Electronics". ACS Nano 9 (2015) 3421–3427.

[15] J. Lee, H. Kwon, J. Seo, S. Shin, J.H. Koo, C. Pang, S. Son, J.H. Kim, Y.H. Jang, D.E. Kim and T. Lee, "Conductive Fiber-Based Ultrasensitive Textile Pressure Sensor for Wearable Electronics". Adv. Mater. 27 (2015) 2433–2439.

[16] G. Hossain, I. Z. Hossain, and G. Grabher, "*Piezoresistive smart-textile sensor for inventory management record*". Sensors and Actuators A: Physical, volume 315, issue 112300, 2020.

[17] Z. Tang, D. Yao, S. Hu, D. Du, W. Shao, B Tang, J. Fan, X. Tang and J. Gao, "Highly conductive, washable and super-hyperbolic wearable carbon nanotubes e-textile for vacuum pressure sensors". Sensors and Actuators A: Physical, volume 303, issue 111710, 2020.

[18] C. Legner, U. Kalwa, V. Patel, A. Chesmore, and S. Pandey, "Sweat sensing in the smart wearable ear: Towards integrative, multifunctional and body-complaint perspiration analysis". Sensors and Actuators A: Physical, volume 296, pp: 200 – 221, 2019.

[19] A. Chauraya, W. Whittow, J. Vardaxoglou, Y. Li, R. Torah, K. Yang, S. Beeby and J. Tudor, "Inkjet Printed Dipole Antennas on Textiles for Wearable Communications". IET Microwaves, Antennas & Propagation, Volume 7, Issue 9, June 2013, Pages 760–767, DOI: 10.1049/iet-map.2013.0076.

[20] X. Huang, T. Leng, M. Zhu, X. Zhang, J.C. Chen, K. Chang, M. Aqeeli, A.K. Geim, K.S. Novoselov and Z. Hu, "Highly Flexible and Conductive Printed Graphene for Wireless Wearable Communications Applications". Scientific Reports 5, Article number 18298, (2015), doi:10.1038/srep18298.

[21] L. V. Langenhove, "Smart Textiles for Medicine and Healthcare: Materials, Systems and Applications". Woodhead Publishing Limited, 2007.

[22] R. Paradiso, G. Loriga, N. Taccini, A. Gemignani, and B. Ghelarducci, *"WEALTHY – A wearable healthcare system: New frontier on e-textile*". J. Telecommun. Inf. Technol. 4, 105–113 (2005).

[23] T.-H. Kang, C. Merritt, E. Grant, B. Pourdeyhimi and H. Nagle, "*Nonwoven Fabric Active Electrodes for Biopotential Measurement During Normal Daily Activity*". Biomed. Eng. IEEE Trans. on 55 (2008) 188–195.

[24] K. Takei, W. Honda, S. Harada, T. Arie and S. Akita, "Toward Flexible and Wearable Human-Interactive Health-Monitoring Devices". Adv. Healthc. Mater. 4 (2015) 487–500.

[25] M. Liu, T. Ward, D. Young, H. Matos, Y. Wei, J. Adams, and K. Yang, "Electronic textiles based wearable electrotherapy for pain relief". Sensors and Actuators A: Physical, volume 303, issue 111701, 2020.

[26] S. Nasiri, and M. R. Khosravani, "Progress and challenges in fabrication of wearable sensors for health monitoring". Sensors and Actuators A: Physical, volume 312, issue: 112105, 2020.

[27] X. Zhou, C. Hu, X. Lin, X. Han, X. Zhao, and J. Hong, “Polyaniline-coated cotton knitted fabric for body motion monitoring”. Sensors and Actuators A: Physical, volume 321, issue 112591, 2021.

[28] Z. A. Abro, Z. Yi-Fan, H. Cheng-Yu, R. A. Lakho, and C. Nan-Liang, “Development of a smart garment for monitoring body postures based on FBG and flex sensing technologies”. Sensors and actuators A: Physical, volume 272, pp: 153 – 160, 2018.

[29] Mohammad Reza Khosravani, Tamara Reinicke, 3D-printed sensors: Current progress and future challenges, Sensors and Actuators A: Physical, Volume 305, 2020, 111916, ISSN 0924-4247, https://doi.org/10.1016/j.sna.2020.111916.

[30] Hongbo Dai, Erik T. Thostenson, Scalable and multifunctional carbon nanotube-based textile as distributed sensors for flow and cure monitoring, Carbon, Volume 164, 2020, Pages 28-41, ISSN 0008-6223, https://doi.org/10.1016/j.carbon.2020.02.079.

[31] uz Zaman, S., Tao, X., Cochrane, C. et al. Launderability of Conductive Polymer Yarns Used for Connections of E-textile Modules: Mechanical Stresses. Fibers Polym 20, 2355–2366 (2019). https://doi.org/10.1007/s12221-019-9325-x.

[32] Sigrid Rotzler, Christine Kallmayer, Christian Dils, Malte von Krshiwoblozki, Ulrich Bauer & Martin Schneider-Ramelow (2020) Improving the washability of smart textiles: influence of different washing conditions on textile integrated conductor tracks, The Journal of The Textile Institute, 111:12, 1766-1777, DOI: 10.1080/00405000.2020.1729056.

[33] M. Yazdan Mehr, W.D. van Driel, S. Koh, G.Q. Zhang, Reliability and optical properties of LED lens plates under high temperature stress, Microelectronics Reliability, Volume 54, Issue 11, 2014, Pages 2440-2447, ISSN 0026-2714, https://doi.org/10.1016/j.microrel.2014.05.003.

[34] A. R. Ochana, D. A. Hutt, D. C. Whalley, F. Sarvar and A. Al-Habaibeh, "Modeling of the Power Cycling Performance of a Si on Si Flip Chip Assembly," Thermal and Thermomechanical Proceedings 10th Intersociety Conference on Phenomena in Electronics Systems, 2006. ITHERM 2006., 2006, pp. 243-250, doi: 10.1109/ITHERM.2006.1645349.

[35] Ephraim Suhir (2019) Analytical thermal stress modelling in electronics and photonics engineering: Application of the concept of interfacial compliance, Journal of Thermal Stresses, 42:1, 29-48, DOI: 10.1080/01495739.2018.1525331.

[36] R. Hui, “*Photo-Electro-Thermal Theory for LED Systems: Basic Theory and Applications*”, Cambridge University Press, 2017.

[37] S. Yaseen, A. Al-Habaibeh, D. Su, F. Othman, Real-time crowd density mapping using a novel sensory fusion model of infrared and visual systems, Safety Science, Volume 57, 2013, Pages 313-325, ISSN 0925-7535, https://doi.org/10.1016/j.ssci.2013.03.007.

[38] B. Yang, Y. Huang, and L. Cheng, “Defect Detection and Evaluation of Ultrasonic Infrared Thermography for Aerospace CFRP Composites”. Infrared Physics & Technology. Volume 60, September 2013, Pages 166-173, https://doi.org/10.1016/j.infrared.2013.04.010.

[39] Asrar, M., Al-Habaibeh, A. And Houda, M., 2016. Innovative Algorithm To Evaluate The Capabilities Of Visual, Near Infrared, And Infrared Technologies For The Detection Of Veins For Intravenous Cannulation. Applied Optics, 55 (34), D67-D75. Issn 0003-6935.

[40] B.B. Lahiri, S. Bagavathiappan, T. Jayakumar and J. Philip, “Medical Applications of Infrared Thermography: A Review”. Infrared Physics & Technology. Volume 55, Issue 4, July 2012, Pages 221-235, https://doi.org/10.1016/j.infrared.2012.03.007.

[41] HAWAS, A. and AL-HABAIBEH, A., 2020. An innovative approach towards enhancing energy conservation in buildings via public engagement using DIY infrared thermography surveys. Energy and Built Environment.

[42] J. P.de Brito Filho and J. R.Henriquez, “Infrared Thermography Applied for High-Level Current Density Identification Over Planer Microwave Circuit Sectors”. Infrared Physics & Technology, Volume 53, March 2010, Pages 84 – 88, https://doi.org/10.1016/j.infrared.2009.09.010.

[43] Al-Habaibeh, A., Shi, F., Brown, N., Kerr, D., Jackson, M. And Parkin, R.M., 2004. A Novel Approach For Quality Control System Using Sensor Fusion Of Infrared And Visual Image Processing For Laser Sealing Of Food Containers. Measurement Science And Technology, 15 (10), Pp. 1995-2000. Issn 0957-0233; 1361-6501.

[44] Elgargni, M., Al-Habaibeh, A. And Lotfi, A., 2015. Cutting Tool Tracking And Recognition Based On Infrared And Visual Imaging Systems Using Principal Component Analysis (Pca) And Discrete Wavelet Transform (Dwt) Combined With Neural Networks. The International Journal Of Advanced Manufacturing Technology, 77 (9), Pp. 1965-1978. Issn 0268-3768.

[45] S. Bagavathiappan, B.B. Lahiri, T. Saravanan, John Philip and T.Jayakumar, "Infrared Thermography for Condition Monitoring – A Review". Infrared Physics & Technology, Volume 60, September 2013, Pages 35-55, https://doi.org/10.1016/j.infrared.2013.03.006.

[46] C. Meola, S. Boccardi and G. M. Carlomagno, "Measurements of Very Small Temperature Variations with LWIR QWIP Infrared Camera". Infrared Physics & Technology, Volume 72, September 2015, Pages 195 – 203, https://doi.org/10.1016/j.infrared.2015.08.004.

[47] M. J. Moran, H. N. Shapiro, B. R. Munson and D. P DeWitt, "Introduction to thermal Systems Engineering", ISBN: 978 – 0 – 471 – 20490 – 9, 2003.

[48] D. W. Mackowski, "Conduction Heat Transfer, Notes for MECH 7210". Mechanical Engineering Department, Auburn University. URL: http://www.eng.auburn.edu/~dmckwski/mech7210/condbook.pdf.

[49] T. Pang, "An Introduction to Computational Physics", Cambridge university Press, ISBN: 9780511800870, 2012.

[50] I-H. Tan, G. L. Snider, L. D. Chang and E. L. Hu, "A Selfconsistent Solution of Schrodinger-Poisson Equations Using a Non-Uniform Mesh". Journal of Applied Physics, 68(4071), 1990.

[51] M. M. Khader and A. M. Megahed, "Numerical Simulation Using the Finite Difference Method for The Flow and Heat Transfer in a Thin Liquid Film Over an Unsteady Stretching Sheet in A Saturated Porous Medium in The Presence of Thermal Radiation". Journal of King Saud University – Engineering Sciences, Volume 25, Issue 1, January 2013, Pages 2 – 34, https://doi.org/10.1016/j.jksues.2011.10.002.

[52] H. Wu, X. Li and Y. He, "A New Couples Explicit Finite Difference Model for Wellbore Flow and Heat Transfer in CO2 Geological Storage". Energy Procedia, Volume 114, July 2017, Pages 3597 – 3606, https://doi.org/10.1016/j.egypro.2017.03.1491.

[53] Y. Zhu, H. Liao and C. Coddet, "Transient Thermal Analysis and Coating Formation Simulation of Thermal Spray Process by Finite Difference Method". Surface and Coatings Technology, Volume 200, Issue 16 – 17, April 2006, Pages 4665 – 4673. https://doi.org/10.1016/j.surfcoat.2004.10.100.

[54] K. Speicher, A. Steinboeck, T. Kiefer and A. Kugi, "Modelling Thermal Shocks and Air Cooling Using the Finite Difference Method". IFAC Proceedings Volumes, Volume 45, Issue 2, 2012, Pages 364 – 368. https://doi.org/10.3182/20120215-3-AT-3016.00064.

[55] Ch. Maierhofer, H. Wiggenhauser, A. Brink and M. Röllig, "Quantitative Numerical Analysis of Transient IR- Experiments on Building". Infrared Physics & Technology, Volume 46, Issues II.1 -2, December 2004, Pages 173 – 180. https://doi.org/10.1016/j.infrared.2004.03.022.

[56] D. D. Burleigh, "Bibliography of the Application of Infrared Thermography to Electronic and Microelectronic Circuits", in Thermosense X, Proceedings of SPIE Vol. 0934, 1988, pp. 97-100.

[57] R. Lehtiniemi, "Bibliography of the Application of Infrared Thermography to Electronics", in Thermosense XXI, Dennis H. LeMieux, John R. Snell, Jr., Eds., Proceedings of SPIE Vol. 3700, 1999, pp. 202-208.

[58] Farnell, http://www.farnell.com/datasheets/1446099.pdf, accessed on 10 Dec 2021.

[59] M. Nashed, D. A. Hardy, T. H. Riley, and T. Dias, “A novel method for embedding semiconductor dies within textile yarn to create electronic textiles”. Fibers volume 7, issue 2, 2019.

[60] P. Lugoda, T. H. Riley, C. Oliveira, R. Morris, and T. Dias, “Developing novel temperature sensing garments for health monitoring application”. Fibers, volume 6, issue 3, 2018.

[61] A. Komolafe, R. Torah, Y. Wei, H. Matos, M. Li, D. Hardy, T. Dias, M. Tudor, and S. Beeby, “Integrating flexible filament circuits for e-textile application”. Advanced Materials Technologies, volume 4, issue 7, 2019.

[62] Dymax Corporation ELECTRONIC ASSEMBLY MATERIALS: 9001-E-V3.5 Product Data Sheet: Multi-Cure 9001-E-V3.5 Resilient, Clear Encapsulant. Available online: https://www.dymax.com/images/pdf/pds/ 9001-e-v35.pdf. (Accessed: Friday 07 May 2021).

[63] D. A. Hardy, I. Anastasopoulos, M. –N. Nashed, C. Oliveira, T. Hughes-Riley, A. Komolafe, J. Tudor, R. Torah, S. Beeby, and T. Dias, “Automated insertion of package dies onto wire and into a textile yarn sheath”. Microsyst. Technol. 2019.

[64] D. A. Hardy, Z. Rahemtulla, A. Satharasinghe, A. Shahidi, C. Oliveira, I. Anastasopoulos, M.N. Nashed, M. Kgatuke, A. Komolafe, R. Torah, J. Tudor, T. Hughes-Riley, S. Beeby, and T. Dias, “Wash testing of electronic yarn”, Materials, Volume 13, Number 5, 2020.